Nano Research
2023, 16(2): 3063–3073

ISSN 1998-0124 CN 11-5974/O4
https://doi.org/10.1007/s12274-022-5043-6

Research Article

Introduction of graphene oxide-supported multilayer-quantum dots nanofilm into multiplex lateral flow immunoassay: A rapid and ultrasensitive point-of-care testing technique for multiple respiratory viruses

Wenqi Wang[1,2,§], Xingsheng Yang[1,§], Zhen Rong[1,§], Zhijie Tu[1], Xiaochang Zhang[1], Bing Gu[3] (✉), Chongwen Wang[1,2,3] (✉), and Shengqi Wang[1] (✉)

[1] *Beijing Institute of Microbiology and Epidemiology, Beijing 100850, China*
[2] *College of Life Sciences, Anhui Agricultural University, Hefei 230036, China*
[3] *Laboratory Medicine, Guangdong Provincial People's Hospital, Guangdong Academy of Medical Sciences, Guangzhou 510000, China*
[§] *Wenqi Wang, Xingsheng Yang, and Zhen Rong contributed equally to this work.*

Received: 3 August 2022 / **Revised:** 9 September 2022 / **Accepted:** 11 September 2022

ABSTRACT

A lateral flow immunoassay (LFA) biosensor that allows the sensitive and accurate identification of severe acute respiratory syndrome coronavirus 2 (SARS-CoV-2) and other common respiratory viruses remains highly desired in the face of the coronavirus disease 2019 pandemic. Here, we propose a multiplex LFA method for the on-site, rapid, and highly sensitive screening of multiple respiratory viruses, using a multilayered film-like fluorescent tag as the performance enhancement and signal amplification tool. This film-like three-dimensional (3D) tag was prepared through the layer-by-layer assembly of highly photostable CdSe@ZnS-COOH quantum dots (QDs) onto the surfaces of monolayer graphene oxide nanosheets, which can provide larger reaction interfaces and specific active surface areas, higher QD loads, and better luminescence and dispersibility than traditional spherical fluorescent microspheres for LFA applications. The constructed fluorescent LFA biosensor can simultaneously and sensitively quantify SARS-CoV-2, influenza A virus, and human adenovirus with low detection limits (8 pg/mL, 488 copies/mL, and 471 copies/mL), short assay time (15 min), good reproducibility, and high accuracy. Moreover, our proposed assay has great potential for the early diagnosis of respiratory virus infections given its robustness when validated in real saliva samples.

KEYWORDS

lateral flow immunoassay, multilayered film-like quantum dots (QDs), simultaneous detection, respiratory viruses, severe acute respiratory syndrome coronavirus 2 (SARS-CoV-2)

1 Introduction

Since December 2019, the coronavirus disease 2019 (COVID-19) pandemic has inflicted massive health and economic damages, including over 5 million deaths, heavy personal and societal healthcare burden, and long-term economic stagnation, worldwide [1]. Severe acute respiratory syndrome coronavirus 2 (SARS-CoV-2) is the causative agent of COVID-19 and it spreads primarily through the respiratory tract via droplets and aerosols [2, 3]. The early clinical symptoms (e.g., coughing, fever, and difficulty breathing) caused by SARS-CoV-2 are similar to those induced by common respiratory viruses, such as influenza A virus (FluA), influenza B virus (FluB), and human adenovirus (HAdV) [4, 5]. Notably, many countries have reported high numbers of SARS-CoV-2 cases with FluA H1N1 or HAdV coinfection [6]. Recent studies have also confirmed that SARS-CoV-2 coinfected with other respiratory viruses worsens the severity of COVID-19 and increases mortality rate [7, 8]. Hence, the timely and accurate detection of SARS-CoV-2 and other common respiratory viruses in the early stages of virus infection is the key for effective treatment, avoiding misdiagnosis, and minimizing losses. Current mature detection methods for viruses, such as real-time reverse transcription-polymerase chain reaction (RT-PCR), nucleotide sequencing, and enzyme-linked immunosorbent assay (ELISA), require tedious procedures and large instruments for result output or RNA extraction through lysing virions prior to testing [9–11]. These methods are thus expensive, laborious, and time-consuming. Therefore, a facile analytical technique that can support the rapid and sensitive on-site detection of respiratory viruses is urgently needed.

Given its distinct characteristics, including rapidity, user-friendliness, portability, low cost, and multitarget detection ability, lateral flow immunoassay (LFA) has been considered as the most promising point-of-care testing (POCT) technology and is widely used in clinical inspection, personal health self-checking, and food safety monitoring [12–15]. In theory, the LFA-based virus antigen detection kit is a good choice for the rapid screening of SARS-CoV-2 and other common respiratory viruses because of its

Address correspondence to Shengqi Wang, sqwang@bmi.ac.cn; Chongwen Wang, wangchongwen1987@126.com; Bing Gu, gb20031129@163.com

following advantages: (i) It does not require professional operators and can be widely used at different sites, such as hospitals, community medical institutions, airports, stations, schools, and homes. (ii) It can provide testing results directly and rapidly (generally < 20 min) without the use of complicated instruments. (iii) LFA technique can analyse multiple targets in a single test by setting multiple test lines on one strip that effectively simplifying the detection process [16–18]. However, the current developed LFA methods continue to exhibit limited quantitative ability, low sensitivity (generally > 0.1 ng/mL), and low throughput (≤ 2) in the detection of respiratory viruses because of the inadequate performance (e.g., instability, low signal intensity, poor dispersion, or large size) of traditional sphere nanotags and the complex compositions of respiratory tract samples (e.g., saliva, throat swabs, and sputum) [19–21]. To date, although many colloidal Au NPs-based LFA kits and LFA technologies with enhanced sensitivity, including fluorescence-based, chemiluminescence-based, and Raman signal-based strategies, have been proposed for SARS-CoV-2 detection, these methods remain incapable of simultaneously and sensitively detecting multiple respiratory viruses. A novel LFA system with improved signal amplification capability, immune binding efficiency, and stability should be developed to meet the demand of the multiplex detection of respiratory viruses.

In recent years, two-dimensional (2D) film-type nanomaterials, such as graphene and its derivatives, molybdenum disulfide, and black phosphorus, have demonstrated enormous potential in the rapid diagnostic field due to their unique structural features (e.g., large surface area, ultrathin structure, and abundant surface active groups) and extraordinary electronic and optical properties [22–25]. For example, Merkoçi's group and Gao's group respectively reported that graphene oxide (GO) nanosheets and black phosphorus are high-performance film-type signal nanotags that can effectively improve the sensitivity of LFA [26, 27]. Moreover, our recently published work demonstrated that quantum dots (QDs) loaded onto GO nanosheets combine the advantages of QDs and GO nanosheets, including 2D structure, high photostability, and strong luminescence, and can be used as flexible fluorescent nanotags to construct a LFA system for bacterial detection [28]. Inspired by these works, herein, we propose a GO-based three-dimensional (3D) fluorescent nanosheet with a triple-layer QD shell (GO@TQD) and introduced it into a LFA strip to enable the rapid, ultrasensitive, and quantitative analysis of multiple respiratory viruses by a single test.

The proposed assay has two great advantages over previous LFA techniques for viruses. First, the 3D GO@TQD nanofilm, which is reported here for the first time, consists of three components from the inside to the outside: (i) a 2D monolayer GO nanosheet that acts as a massive and flexible inner supporter, (ii) three layers of polyetherimide (PEI) that greatly improve the dispersibility of the nanosheets and effectively adsorb numerous carboxylated QDs, and (iii) three layers of QD shells containing thousands of carboxylated QDs that generate fluorescence signals that are thousands of times larger than those generated by a single QD and provide numerous surface sites for antibody conjugation. The novel film-like fluorescent tag (GO@TQD) exhibits a larger surface area, superior fluorescence properties, and better dispersibility and stability than the commonly used spherical fluorescent materials for LFA application, thus greatly improving the detection sensitivity of the test strip. Second, our constructed multiplex LFA system allows the on-site and simultaneous detection of SARS-CoV-2, FluA, and HAdV within 15 min. To our knowledge, we are the first to report the direct and multiplex detection of three respiratory viruses on one LFA strip. The limits of detection (LODs) of the proposed assay are 100 and 12.5 times more sensitive than those of conventional colorimetric-based LFA and ELISA, respectively. Moreover, the GO@TQD-based fluorescence LFA exhibits excellent stability, specificity, and accuracy when used to detect real respiratory tract samples, thus showing great potential for POCT applications.

2 Experimental section

2.1 Preparation of GO@TQD nanofilm

Materials, reagents, and instrumentation used in this study were described in Section S1.1 in the Electronic Supplementary Material (ESM). As shown in Scheme 1(a), GO@TQD nanofilms were synthesized by using the layer-by-layer (LBL) self-assembly strategy based on electrostatic interaction. First, 1 mL of monolayer GO nanosheet solution (2 mg/mL) was diluted twice with deionized water and sonicated for 10 min for uniform dispersion. The solution was centrifuged (14,000 rpm, 10 min) to discard the supernatant containing small GO fragments (< 200 nm), and the precipitate was then resuspended in 30 mL of deionized water to obtain 200–500 nm GO nanosheets [29]. This solution was then added with 1 mL of PEI (1 mg/mL) and sonicated intensely for 30 min. After the reaction, the PEI-coated GO (GO@PEI) sheets were separated through centrifugation at 14,000 rpm for 8 min. The excess PEI was washed twice with deionized water, and the precipitate was resuspended in 30 mL of deionized water. Then, the GO@PEI solution was incubated with 0.2 mL of CdSe/ZnS-COOH QDs (0.1 μM) and then sonicated for 60 min. The GO@QD nanofilms were obtained by washing once by centrifugation (7,000 rpm, 8 min) to remove excess QDs and then resuspended in 30 mL of deionized water. Finally, the above steps were repeated to obtain GO@double QD shell layers (DQD) nanosheets with two layers of QDs and GO@TQD nanofilms with three layers of QDs successively. Subsequently, the prepared GO@TQD nanofilms were centrifuged at 5,500 rpm for 8 min and stored in 20 mL of ethanol.

2.2 Preparation of antibody-modified GO@TQD tags

The monoclonal antibodies of the three target respiratory viruses were conjugated with GO@TQD nanofilms through carbodiimide chemistry. First, 1 mL of GO@TQD nanofilms were separated from ethanol, resuspended in 0.5 mL of 0.1 M 2-(N-morpholino) ethanesulfonic (MES) buffer (pH = 6.0), and then mixed with 5 μL of 0.1 M EDC and 10 μL of 0.1 M NHS. After ultrasonic activation for 15 min, the activated GO@TQD nanofilms were collected through centrifugation (5,500 rpm, 6 min) and resuspended in 0.5 mL of 10 mM phosphate-buffered saline (PBS) solution (pH 7.4). Then, the activated GO@TQD was incubated with 8 μg of SARS-CoV-2, HAdV, or H1N1 antibodies for 2 h, and blocked with 100 μL of 10% bovine serum albumin (BSA) solution for another 1 h. Finally, the immuno-GO@TQD nanofilms were washed once with PBS (10 mM) through centrifugation (5,500 rpm, 6 min) and resuspended in 0.5 mL of PBS (10 mM, pH 7.4) storage solution containing 0.02% NaN_3 (w/v) and 1% BSA (w/v).

2.3 Preparation of the multiplexed LFA strip

The LFA strip was constructed in the form of a three-channel detection platform from a sample pad, a conjugate pad, a NC membrane containing three test lines and a control line, and an absorbent pad (Scheme 1(b)). The detection antibodies of SARS-CoV-2 (1.4 mg/mL), HAdV (1.2 mg/mL), and H1N1 (1.2 mg/mL) were sprayed on the test line 1 (T1), test line 2 (T2), and test line 3 (T3), respectively, to capture target immuno-GO@TQD–virus

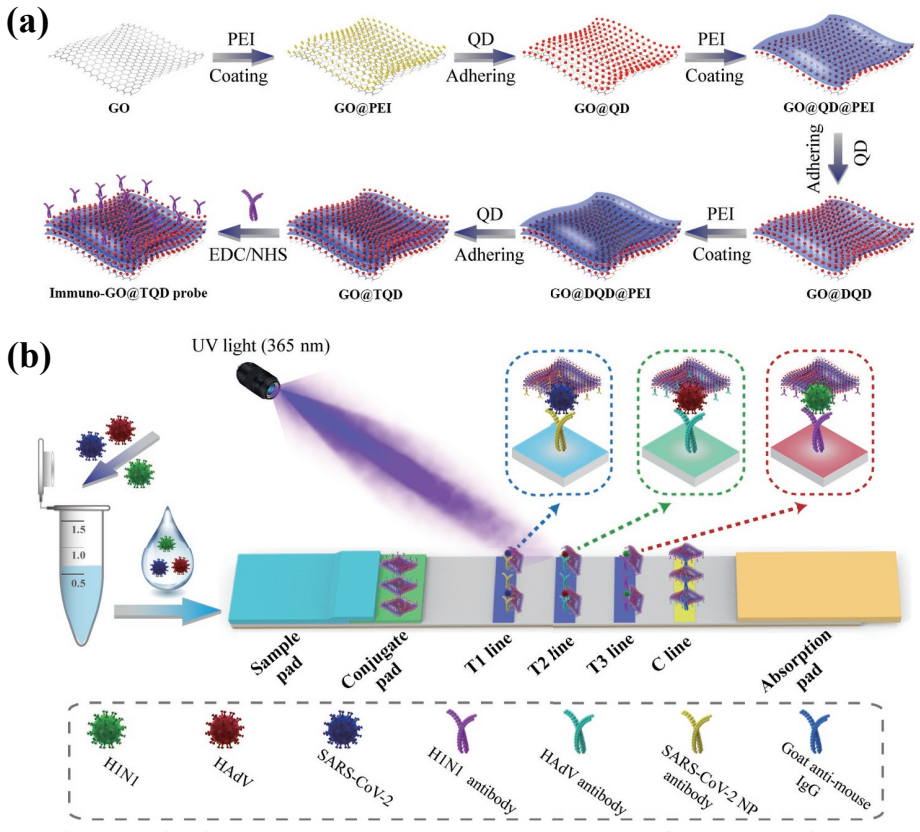

Scheme 1 Schematic of (a) the fabrication of the film-like GO@TQD nanoprobe and (b) GO@TQD-based fluorescence LFA for the direct and simultaneous analysis of SARS-CoV-2, H1N1, and HAdV.

complexes. Goat anti-mouse IgG (0.5 mg/mL) was sprayed on the control line to bind excess immuno-GO@TQD labels. Then, the prepared NC membrane was placed in a drying oven at 37 °C for 2 h. The immuno-GO@TQD tag was bound to the conjugate pad by using the vacuum freeze dryer LGJ-10C. All the components were assembled on a plastic backing card, and the LFA card was cut into 3 mm strips for further use.

2.4 Analytical procedure for simultaneous detection of three respiratory viruses

HAdV and FluA H1N1 virus particles were inactivated through continuous heating in a drying oven at 55 °C for 20 min. Then, the exact concentrations of the H1N1 and HAdV samples were quantified through microdrop digital PCR (dd PCR). As shown in Fig. S1 in the ESM, the initial concentrations of the HAdV and H1N1 samples were 8.539×10^8 and 4.115×10^8 copies/mL, respectively. The samples of SARS-CoV-2 nucleocapsid protein (NP), HAdV, and H1N1 viruses were diluted into different concentration gradients of 0–10 ng/mL, 0–10^6 copies/mL, and 0–10^6 copies/mL with PBS (10 mM), respectively. Next, a mixture of 40 μL of virus sample and 40 μL of the running buffer (10 mM PBS, 1% Tween 20, 5% fetal bovine serum (FBS), 1% NP-40, and 5% BSA) was prepared and added onto the sample pad for 15 min of chromatographic reaction. The fluorescence signals of three T lines were recorded with a commercial fluorescent reader under 365 nm excitation.

2.5 Detection of inactivated SARS-CoV-2 and real biological samples

Different concentrations of SARS-CoV-2 NP antigen (0.1–5 ng/mL), HAdV (10^4–5×10^5 copies/mL), and H1N1 (10^4–5×10^5 copies/mL) virus samples were added into real saliva samples from healthy volunteers. The mixtures were tested by the established GO@TQD-LFA detection platform, and the recovery (%) of the three target respiratory viruses (SARS-CoV-2, HAdV, and H1N1) in saliva specimens was calculated from the established calibration curves. Inactivated SARS-CoV-2 virus samples were detected at different dilutions (2,000–512,000 times) by using the established GO@TQD-LFA method. Calibration curves were plotted from fluorescence values, and used for determination of inactivated SARS-CoV-2 samples with unknown concentrations.

3 Results and discussion

3.1 Principle of film-like GO@TQD-based fluorescence LFA

Herein, we designed and introduced the film-like GO@TQD nanoprobe into the LFA platform as an alternative to conventional spherical fluorescent microspheres. Our nanoprobe can confer prominent characteristics to LFA, including (i) a GO@based film-type structure with a massive surface area and colloidal stability, (ii) three layers of PEI/QD shells containing thousands of carboxylated QDs for the superior generation of fluorescence and excellent dispersibility, and (iii) numerous antibodies modified onto the outermost layer for capturing target viruses efficiently and specifically. With these advantages of film-like GO@TQD tags, a multiplex and ultrasensitive fluorescence LFA platform for multiple respiratory viruses can be constructed.

The operating principle of GO@TQD-LFA for the simultaneous screening of SARS-CoV-2, HAdV, and H1N1 is schematically presented in Scheme 1(b). The NP antigen of SARS-CoV-2 has been proven more conserved than other structural proteins including Spike antigen [30, 31]. Previous studies have demonstrated that highly sensitive and specific detection of SARS-CoV-2 can be achieved by using NP as target antigen [32–34]. Thus, we chose NP as target for SARS-CoV-2 detection. The test

specimen was mixed with running buffer and then dropped on the sample pad to initiate LFA detection. In the absence of the target virus in the solution, the added GO@TQD nanoprobes flowed through the three test lines and were immobilized by the goat anti-mouse IgG antibody precoated on the control zone. When the solution contained one or more of the target viruses, the formed GO@TQD–virus complexes were specifically identified and captured by the anti-SARS-CoV-2/HAdV/H1N1 antibodies on the T1/T2/T3 lines, and distinct red fluorescence signals were generated under 365 nm ultraviolet (UV) irradiation. The detailed fluorescence intensity values of the three test lines were simultaneously measured by using a commercial fluorescence reader and used for the quantitative analysis of viruses.

3.2 Preparation and characterization of GO@TQD nanofilm

We adopted a PEI-mediated LbL assembly method to fabricate multilayered GO@TQD nanofilms. This method involves the repeated electrostatic adsorption of positively charged PEI and electronegative carboxylated QDs onto the surfaces of GO nanosheets. Notably, the CdSe/ZnS-MPA QDs were chosen as the fluorescent component to construct GO@TQD nanofilm due to their stable fluorescence properties and abundant surface carboxyl groups of the MPA-modified shell for subsequent antibody coupling. The diameter of CdSe/ZnS-MPA QDs was about 15 nm, as revealed in Fig. S2 in the ESM. The CdSe/ZnS-MPA QDs are widely used to build QD-based fluorescent microspheres (e.g., SiO_2@QD and Fe_3O_4@QD) for LFA methods [35–37]. The structure and surface morphology of the GO-based QD nanofilms were characterized through transmission electron microscopy (TEM) and scanning electron microscopy (SEM). The used monolayer GO is a typical extra-thin monodisperse 2D nanosheet (Fig. 1(a)) and can thus act as a flexible and stable film-like supporter and provide a large surface area for QD loading. Branched PEI is a cationic macromolecular polymer that can firmly self-assemble onto the surfaces of electronegative GO nanosheets under sonication [38, 39]. The increase in the zeta potential value of GO@PEI from −52.3 to 39.2 mV confirmed that the PEI layer had been successfully coated onto GO surfaces (Fig. S3 in the ESM). The abundant amino groups of the PEI layer allowed the efficient adsorption of carboxylated CdSe/ZnS QDs onto the GO@PEI surface, thus forming the dense QD-coated GO nanofilm (GO@QD). The TEM image in Fig. 1(b) clearly shows that the as-prepared GO@QDs adsorbed numerous QDs on their surfaces and remained monodispersed. The second PEI layer was then coated onto GO@QD surfaces to provide sufficient positive charges to drive the LBL assembly of the second layer of QDs. By using this strategy, multiple layers of PEI and carboxylated QDs can be subsequently assembled onto the GO surface. The

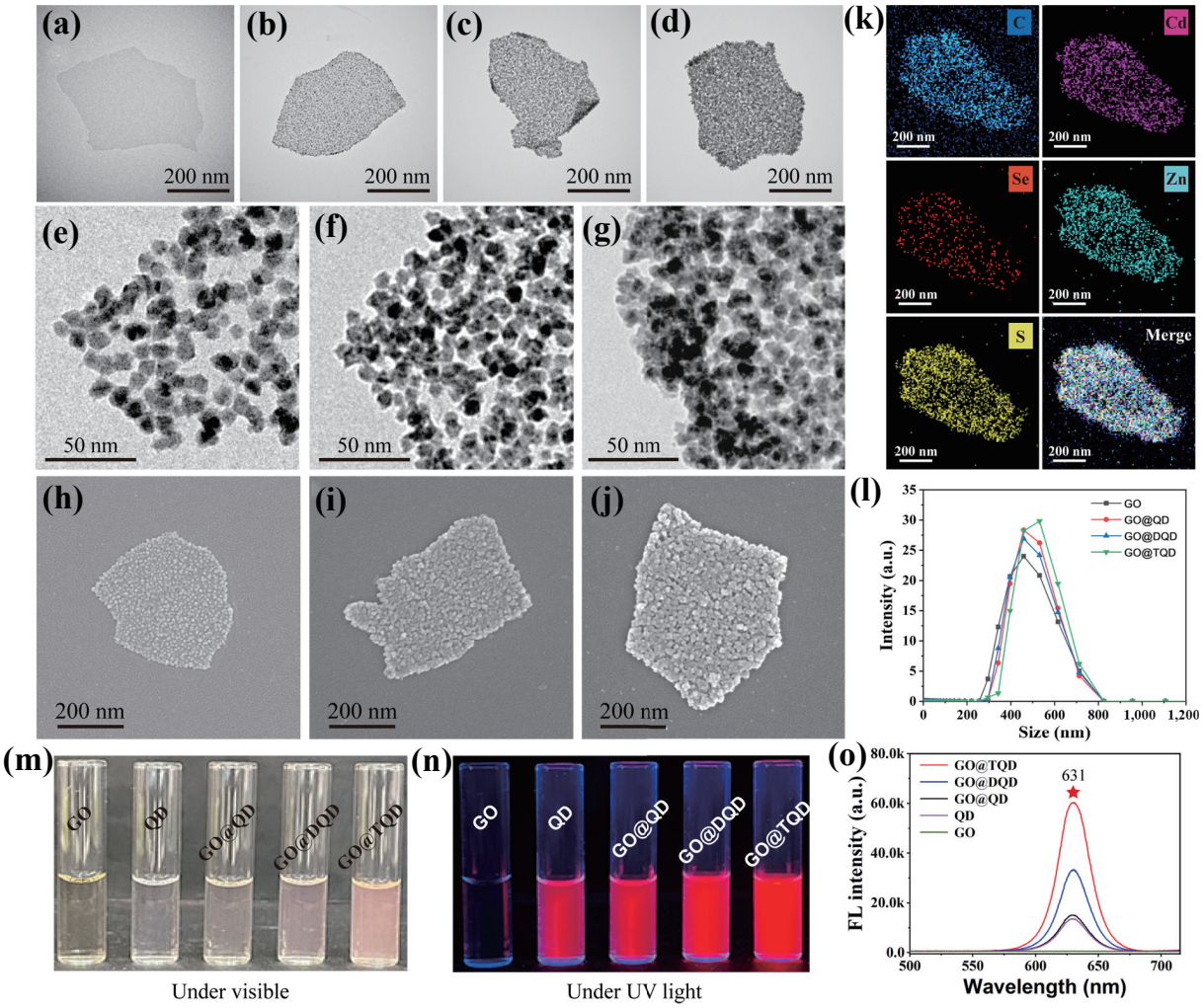

Figure 1 Structural characterization of the prepared GO@TQD nanofilm. TEM images of (a) GO, (b) GO@QD, (c) GO@DQD, and (d) GO@TQD nanofilms. Enlarged TEM images of (e) GO@QD, (f) GO@DQD, and (g) GO@TQD nanofilms. SEM images of (h) GO@QD, (i) GO@DQD, and (j) GO@TQD nanofilms. (k) EDS elemental maps of C, Cd, Se, Zn, and S signals on a single GO@TQD nanofilm. (l) Dynamic light scattering distribution of GO, GO@QD, GO@DQD, and GO@TQD. The *x*- and *y*- coordinate represent the size (nm) of the nanofilms and the relative signal intensity, respectively. (m) and (n) Photographs and (o) fluorescence emission spectra of GO, QD, GO@QD, GO@DQD, and GO@TQD nanofilms.

fabricated GO@QDs with double QD shell layers (GO@DQD) and GO@QD with triple QD shell layers (GO@TQD) are presented in Figs. 1(c) and 1(d), respectively. Numerous 15 nm CdSe/ZnS QDs were distributed on the surfaces of GO@TQDs as evident in the magnified TEM images in Figs. 1(e)–1(g). The SEM images (Figs. 1(h)–1(j)) clearly displayed the rough surface morphologies of GO@QD, GO@DQD, and GO@TQD. Obviously, as the layers of the QD shells were increased, the density and amounts of the QDs that adhered onto the GO sheets were greatly increased. Moreover, the dynamic light scattering (DLS) results showed that the hydrodynamic sizes of the GO and QD-coated GO nanofilms were all distributed within the range of 400–600 nm, which indicated that the multilayer QDs coating did not affect the film-like structure of the GO sheets (Fig. 1(l)). The energy dispersive X-ray spectroscopy (EDS) mapping results (Fig. 1(k)) and the EDS spectrum (Fig. S4 in the ESM) of the GO@TQD nanofilm further showed that strong Cd (purple), Se (red), Zn (cyan), and S (yellow) signals from CdSe/ZnS QDs were distributed on the outside of the C (blue) nanofilm, demonstrating that a homogeneous 3D film-like structure was successfully constructed. We roughly calculated the amounts of QDs loaded on the GO@TQD surface (Section S2 and Fig. S5 in the ESM) and found that the maximum QD loading amounts of GO@QD, GO@DQD, and GO@TQD were 1,422, 2,844, and 5,688, respectively.

In addition, the proposed GO@TQD exhibited superior fluorescence performance over common commercial QD (~ 15 nm), GO@QD, and GO@DQD nanofilms (Figs. 1(m) and 1(n)) because of the integration of thousands of QDs into one nanofilm. By comparing the fluorescence intensities of the main emission peaks at ~ 631 nm, we discovered that the luminous ability of GO@TQD was 4.48, 4.03, and 1.81 times higher than that of commercial QDs, GO@QD, and GO@DQD, respectively (Fig. 1(o)). The quantum yield of the GO-based fluorescent nanofilms was further investigated. As shown in Fig. S6 in the ESM, the quantum yield of GO, GO@QD, GO@DQD, and GO@TQD nanofilms was calculated as 0.01%, 23.19%, 47.83%, and 53.74%, respectively. This result verified that the quantum yield of GO@TQD nanofilms increased with increasing of the QD layers.

The stability between GO@TQD nanofilm and commercial QDs was compared, as shown in Fig. 2 and Fig. S7 in the ESM. Obviously, the dispersibility and fluorescence intensity of GO@TQD nanofilm remained stable in high salt solution (0–1,000 mM NaCl) (Fig. 2(a)), whereas the fluorescence signals of commercial QDs decreased after treatment with high concentrations of NaCl (> 100 mM) (Fig. S7(a) in the ESM). In addition, the fabricated GO@TQD nanofilm showed good colloidal stability and strong fluorescence intensity in aqueous solution with the pH levels of 3–14 (Fig. 2(b)), whereas the commercial QDs were severely agglomerated in acidic solution (pH < 6) (Fig. S7(b) in the ESM). Moreover, the fluorescence intensity of commercial QDs starts to decay after 30 days of storage at room temperature (Fig. S7(c) in the ESM). However, no significant change in the fluorescence intensity of GO@TQD was observed after 60 days of storage under the same condition (Fig. 2(c)). These results confirmed that the combination of monodispersed GO nanosheets and hydrophilic PEI/QD layers can guarantee the excellent optical/colloidal stability and dispersibility of the GO@TQD nanofilms in complex environments.

Notably, antivirus antibodies can be directly modified onto the GO@TQD surface via the EDC/NHS-based coupling reaction because the carboxylated QDs had abundant COOH groups [40]. Figure S8 in the ESM shows that the zeta potentials of the immuno-GO@TQD tags for SARS-CoV-2 NP, HAdV, and H1N1 detection were stable at −9.3, −10.7, and −12.5 mV, respectively, when reacted with 8 μg of the capture antibody, indicating that a sufficient amount of antibodies had been modified onto the GO@TQD surface. The Fourier transform infrared (FTIR) spectroscopy results (Fig. S9 in the ESM) also confirmed the successful fabrication of the antibody-conjugated GO@TQD tags. Moreover, the immuno-GO@TQD tags showed stable fluorescence signals that were as strong as those of raw GO@TQD nanofilm at 631 nm by excitation with a 365 nm UV light, indicating that antibody conjugation has no influence on the structural stability and QDs' emission of GO@TQD nanofilm (Fig. S10 in the ESM). The fabricated immuno-GO@TQD tag has the prominent merits of high QD loading amount, excellent stability and monodispersity, and large specific surface areas with numerous reaction sites, and thus can be used as a superior fluorescent nanoprobe to improve the detection performance of LFA.

3.3 Construction of GO@TQD-LFA for multiplex detection of respiratory viruses

Scheme 1(b) depicts the structural design of the GO@TQD-based LFA for the simultaneous detection of three respiratory viruses by using the typical sandwich immunoassay. With its advantageous properties, including high QD loading amount, large specific surface area, numerous reaction sites, and excellent stability and dispersibility, the film-like GO@TQD can be easily introduced

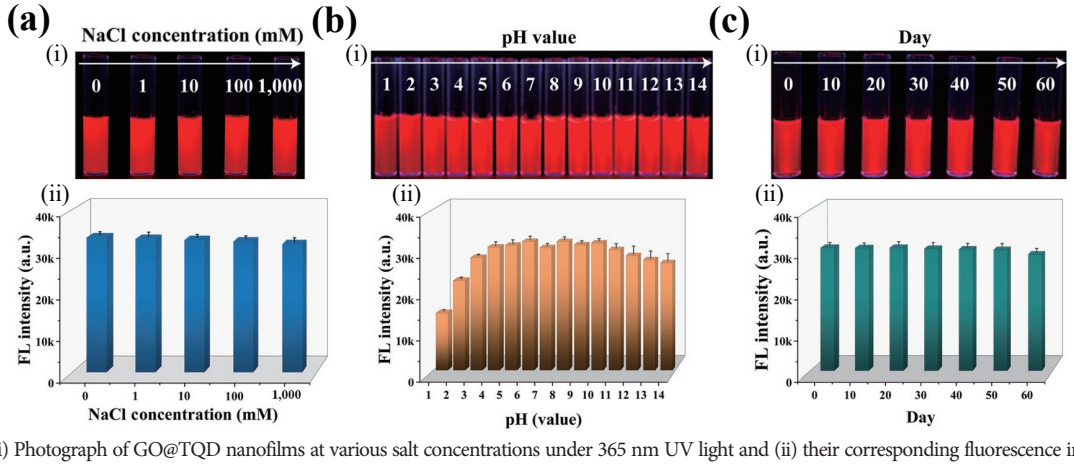

Figure 2 (a) (i) Photograph of GO@TQD nanofilms at various salt concentrations under 365 nm UV light and (ii) their corresponding fluorescence intensities at the maximum emission wavelength. (b) (i) Photographs and (ii) detailed fluorescence signals of GO@TQD nanosheets at various pH levels. (c) (i) Photographs and (ii) detailed fluorescence signals of GO@TQD nanofilms dispersed in ethanol against preservation time.

into the LFA system as a superior fluorescent nanoprobe. The LFA system consisted of a sample pad, a NC membrane with three test lines, one control line, and an absorbent pad. The capture antibodies of SARS-CoV-2 NP, HAdV, and H1N1 were correspondingly dispensed onto the NC membrane to construct three test lines (T1 for SARS-CoV-2, T2 for HAdV, and T3 for H1N1). The selectivities of the three test lines on the multiplex LFA strips for the target viruses were first assessed by testing samples containing SARS-CoV-2 NP (1 ng/mL), HAdV (10^5 copies/mL), and H1N1 (10^5 copies/mL). Figure 3(a)(i) shows the fluorescence photographs of the tested LFA strips. The bright fluorescence bands that had appeared on the corresponding test lines of the LFA strips were consistent with the target viruses present in the samples (strips 1–7). By contrast, all three T lines were not visible in the negative sample (strip 8). The fluorescence signals measured from the T1/T2/T3 lines of the tested strips are displayed in Fig. 3(a)(ii) and clearly presented an on/off pattern in accordance with the different viruses present. These results indicated that the used antibodies have good selectivity and that no cross-reaction occurred on the three test lines. Figures 3(b)(i) and 3(b)(ii) display the interior morphology of the test zones from a positive test and a negative control (no target virus), respectively. These SEM images clearly illustrate the presence of many film-like GO@TQD nanoprobes on the test line for the positive sample and the absence of nanofilms on the same zone for the negative control, thus confirming the reliability of our proposed biosensor.

In theory, increasing the number of QDs integrated into one fluorescent tag increases luminescence, resulting in the increased sensitivity of the fluorescence-LFA method [41–43]. We compared GO@TQD-based LFA and LFA based on other QD tags (GO@QD, GO@DQD, and common QD beads) to verify the effect of the multilayer QDs of the film-like tag on fluorescence signal amplification. Figures 3(c)(i) and 3(c)(ii) present the fluorescence images and measured fluorescence intensities of the tested strips in the QD-LFA, GO@QD-LFA, GO@DQD-LFA, and GO@TQD-LFA groups in the detection of the same concentrations of SARS-CoV-2 NP antigens (0–10 ng/mL). Obviously, the GO@TQD and GO@DQD tags can generate higher fluorescence signals on the test lines of LFA than the common QD beads and GO@QD tags. The red fluorescence signals on the test lines of the QD bead-, GO@QD-, GO@DQD-, and GO@TQD-based LFAs could be observed with the naked eye at the concentrations of 0.5, 0.5, 0.05, and 0.01 ng/mL, respectively. We quantified the fluorescence intensities of all tested strips by using a commercial fluorescent reader and then used these values to draw the calibration curves for the four detection platforms (Fig. 3(d)). The LODs of the QD bead-, GO@QD-, GO@DQD-, and GO@TQD-based LFAs were calculated to be 111, 52, 16, and 8 pg/mL, respectively. These results confirmed that using GO@TQD with many QD layers as the fluorescent tag can effectively improve the detection sensitivity of LFA.

We further optimized the key parameters of the LFA system, including the composition of the running buffer (Fig. S11 in the ESM), the kind of NC membrane (Fig. S12 in the ESM), the

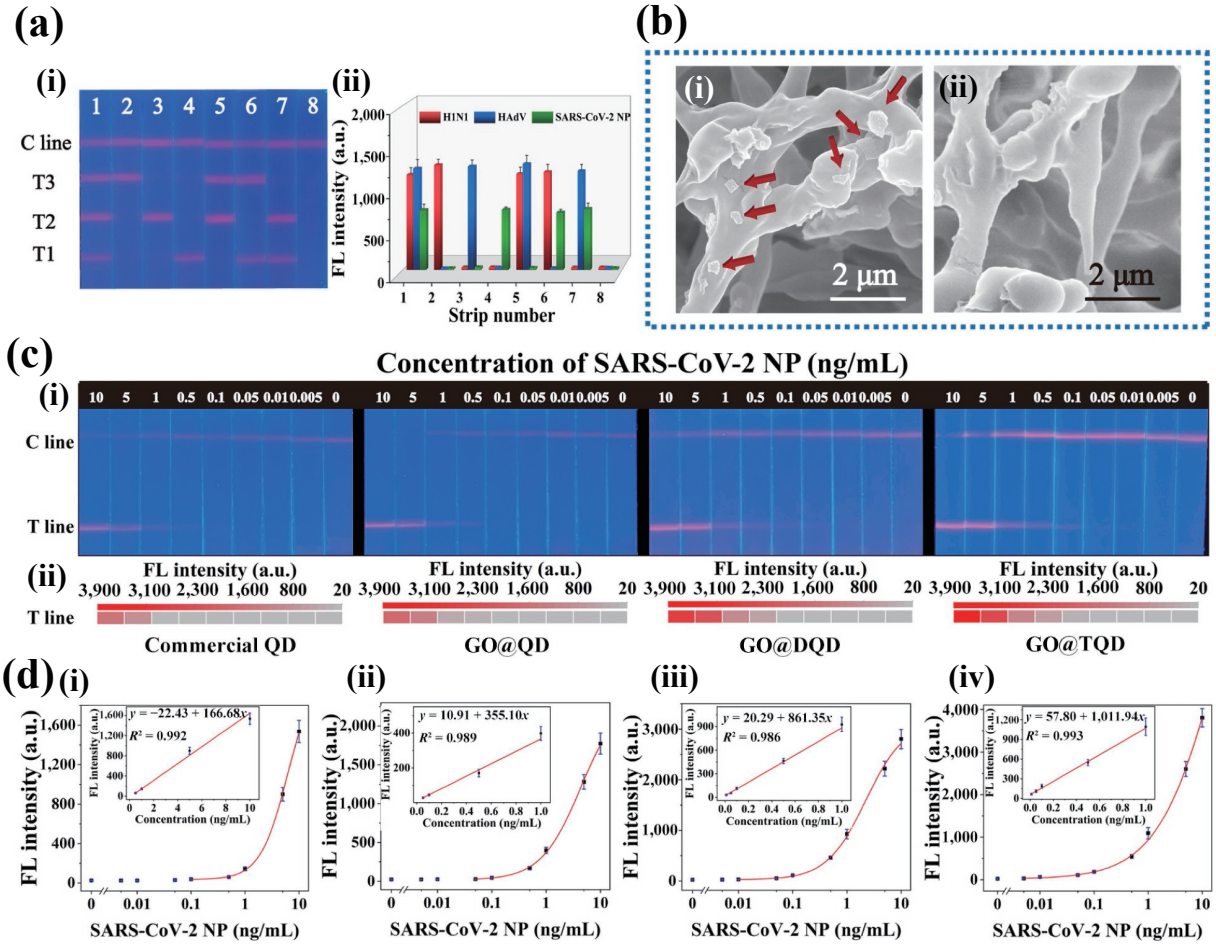

Figure 3 (a) (i) Images and (ii) corresponding fluorescence intensities of GO@TQD-based LFA for evaluating the cross-reactivity of three target respiratory viruses. (b) Typical SEM images of the test line from the (i) positive sample and (ii) blank control. (c) (i) Images and (ii) corresponding fluorescence signals of the T lines of QD bead-LFA, GO@QD-LFA, GO@DQD-LFA, and GO@TQD-LFA strips for SARS-CoV-2 NP detection. (d) Corresponding calibration curves of (i) QD bead-LFA, (ii) GO@QD-LFA, (iii) GO@DQD-LFA, and (iv) GO@TQD-LFA for SARS-CoV-2 NP. Insets show the corresponding linear response of the fluorescence signal to SARS-CoV-2 NP concentration.

concentrations of the detection antibodies sprayed on the test lines (Fig. S13 in the ESM), the dosage of immuno-GO@TQD tags (Fig. S14 in the ESM), and the duration of the chromatographic reaction (Fig. S15 in the ESM) to ensure the best sensitivity and multiplex detection performance for three target viruses. The optimization experiments are described in detail in the Section S3 in the ESM. In brief, we found that running buffer containing 10 mM PBS (pH 7.4), 1% Tween 20, 5% FBS, 1% NP-40, and 5% BSA and 15 min of chromatographic time are suitable for the proposed assay. The CN140 membrane with 10 μm pore size exhibited superior detection performance than other NC membranes on the LFA system and is thus chosen in this study.

3.4 Performance of GO@TQD-based fluorescent LFA in virus detection

To evaluate the power of GO@TQD nanofilm-based LFA for the multiplex detection of respiratory viruses, a series of mixed virus samples containing different concentrations of SARS-CoV-2 NP (0–10 ng/mL), HAdV (0–10^6 copies/mL), and H1N1 (0–10^6 copies/mL) were detected via the proposed assay. Figure 4(a) presents the photographs of the fluorescent strips for the simultaneous detection of the three target respiratory viruses. The fluorescence intensities of the three test lines (T1/T2/T3) gradually diminished with the decrease in the concentrations of the mixed viruses. We found that 50 pg/mL SARS-CoV-2 NP (T1), 1,000 copies/mL HAdV (T2), and 1,000 copies/mL H1N1 (T3) generated the lowest fluorescence signals on the test lines that could be visible to the naked eye. The fluorescence intensity values of the three T lines were quantified by using a commercial fluorescent reader (Fig. 4(b)) and then used to draw the corresponding calibration curves for SARS-CoV-2 NP, HAdV, and H1N1. The sigmoidal calibration curves (Fig. 4(c)) for target viruses exhibited a wide dynamic range and crossed over four orders of magnitude with the correlation coefficients (R^2) of 0.991, 0.993, and 0.990 for SARS-CoV-2 NP, HAdV, and H1N1, respectively. Moreover, GO@TQD-LFA obtained the linearity ranges of 10–500 pg/mL for SARS-CoV-2, 500–10,000 copies/mL for HAdV, and 500–10,000 copies/mL for H1N1 with linear R^2 > 0.988. The LODs of GO@TQD-LFA were calculated as the concentration corresponding to three times the standard deviation of the blank groups (IUPAC protocol) and were approximately 8 pg/mL for SARS-CoV-2 NP, 471 copies/mL for HAdV, and 488 copies/mL for H1N1. We further verified the single-target analysis ability of the proposed LFA system by detecting the samples involving only one kind of respiratory virus. As illustrated in Fig. S16 in the ESM, the detection sensitivity, calibration curves, and sensing range of single-channel analysis based on GO@TQD-LFA were basically consistent with those of the simultaneous detection of three viruses, indicating high independence among the three test lines of our method, as well as stability and accuracy.

We further assessed the reproducibility of the proposed multiplexed LFA through five independent tests. Figure 5(a) displays the detection results of GO@TQD-LFA for high concentrations (10 ng/mL, 10^6 copies/mL, and 10^6 copies/mL), moderate concentrations (1 ng/mL, 10^5 copies/mL, and 10^5 copies/mL), and low concentrations (0.1 ng/mL, 10^4 copies/mL, and 10^4 copies/mL) of mixed SARS-CoV-2/HAdV/H1N1 samples. The fluorescence intensities of LFA strips in each group were fairly uniform with relative standard deviation (RSD) values lower than 8.2%. We further tested other important respiratory viruses, including RSV (10^5 pfu/mL), FluB (10^5 pfu/mL), SARS-CoV NP (10 ng/mL), and MERS-CoV NP (10 ng/mL), by using the prepared LFA strip to verify the specificity of fluorescent LFA based on the film-like GO@TQD. As shown in Fig. 5(b), only the three target viruses can generate bright fluorescence on the corresponding test lines, and all the control groups exhibited a distinct fluorescent band only on the control line. Therefore, GO@TQD-based LFA has excellent specificity for the target respiratory viruses.

By virtue of the superior performance of the film-like GO@TQD, the newly developed LFA method exhibited distinct advantages over traditional immunoassay-based POCT tools, namely, the standard AuNP-based LFA method and ELISA. The details of AuNP-based LFA and ELISA are described in Sections

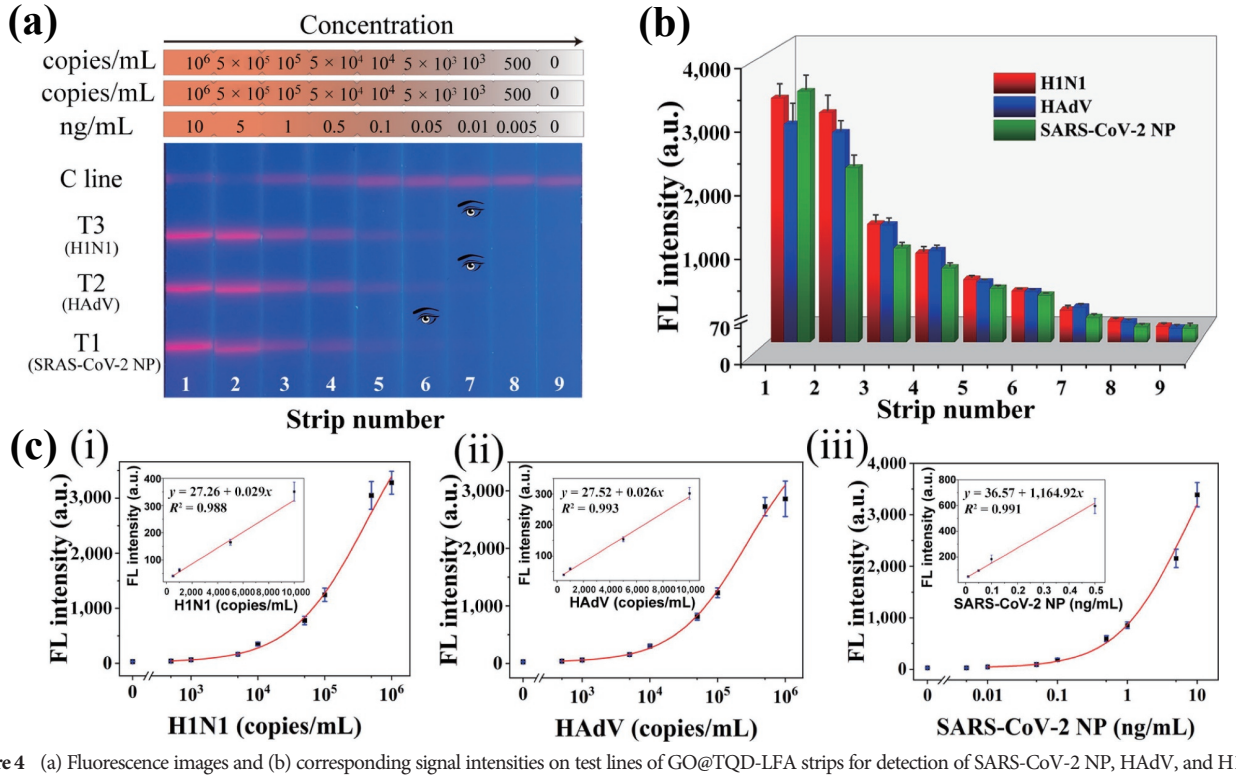

Figure 4 (a) Fluorescence images and (b) corresponding signal intensities on test lines of GO@TQD-LFA strips for detection of SARS-CoV-2 NP, HAdV, and H1N1. (c) Corresponding calibration curves for (i) H1N1, (ii) HAdV, and (iii) SARS-CoV-2 NP.

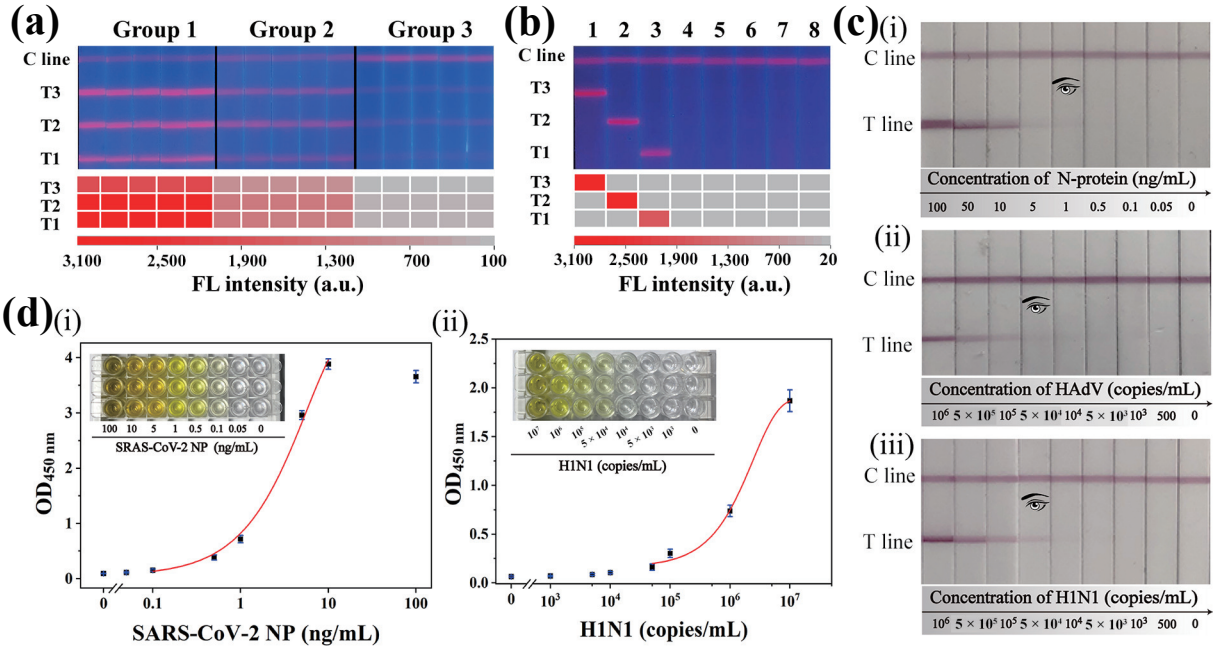

Figure 5 (a) Reproducibility of GO@TQD-LFA for SARS-CoV-2 NP, HAdV, and H1N1. (b) Specificity of GO@TQD-based LFA. Strips 1–8 show the detection results for H1N1 (10^6 copies/mL), HAdV (10^6 copies/mL), SARS-CoV-2 NP (10 ng/mL), RSV (10^5 pfu/mL), FluB (10^5 pfu/mL), SARS-CoV NP (10 ng/mL), MERS-CoV NP (10 ng/mL), and the blank group. (c) Photographs of AuNP-based colorimetric LFA for the detection of different concentrations of (i) SARS-CoV-2 NP, (ii) HAdV, and (iii) H1N1. (d) ELISA for testing of (i) SARS-CoV-2 NP and (ii) H1N1.

S1.2–S1.4 in the ESM. Figures 5(c)(i)–5(c)(iii) show that the LODs based on the colorimetric signal of AuNP-based LFA strips for SARS-CoV-2, HAdV, and H1N1 were 1 ng/mL, 5×10^4 copies/mL, and 5×10^4 copies/mL, respectively. Therefore, compared with that of the AuNP-based LFA, the sensitivity of GO@TQD-LFA had improved by 100 times. The commercially available ELISA kits for SARS-CoV-2 NP antigen (Catalog #KIT40588) and H1N1 (Catalog #KIT11055) were obtained from Sino Biological, Inc. (Beijing, China) and used in accordance with the instructions. As shown in Figs. 5(d)(i) and 5(d)(ii), the LODs of SARS-CoV-2 NP and H1N1 determined by the ELISA kit were 0.1 ng/mL and 5×10^4 copies/mL respectively, which were 12.5 and 100 times higher than those of GO@TQD-LFA, respectively. Apparently, the GO@TQD-LFA can greatly improve sensitivity of existing LFA methods, as well as exhibit excellent ability for multiplex analysis and quantitative detection. In contrast to ELISA, GO@TQD-LFA can avoid tedious operation and quickly complete detection in 15 min with high sensitivity.

3.5 Detection of real biological samples and inactivated SARS-CoV-2

To evaluate the application potential of GO@TQD-LFA for real respiratory tract specimens, we spiked different concentrations of SARS-CoV-2 NP (0.1–5 ng/mL), HAdV (10^4–5×10^5 copies/mL), and H1N1 (10^4–5×10^5 copies/mL) into real saliva specimens from healthy volunteers and directly detected them with the established assay. The saliva specimens were first checked by using RT-PCR to confirm the absence of the target viruses. By calculating the obtained fluorescence signals of each test line, the average recoveries of the proposed GO@TQD-LFA were determined to be 93.1%–100.1% for SARS-CoV-2 NP antigens, 96.1%–108.4% for HAdV-spiked samples, and 91.6%–108.5% for H1N1-spiked samples with coefficients of variation (CV) below 8.11% (Table 1). These results demonstrated that GO@TQD-LFA has excellent accuracy and reliability for the on-site detection of real clinical samples.

The actual capability of GO@TQD-LFA for the rapid identification of SARS-CoV-2 and its variants from other common respiratory pathogens is among our main concerns. We next used our method to test an inactivated SARS-CoV-2 virion solution, which was obtained from Prof. Chengfeng Qin (Beijing Institute of Microbiology and Epidemiology), and determined that its concentration was ~ 2.362×10^8 copies/mL by using dd PCR (Section S1.5 in the ESM). The SARS-CoV-2 inactivated virions were spiked into saliva specimens that were then continuously diluted 2,000–512,000 times and directly loaded onto the GO@TQD-LFA strips. The detection results in Fig. 6(a) clearly demonstrate that the red fluorescence band of the 128,000 times dilution of the inactivated SARS-CoV-2 samples could be still distinguished on the T1 line by visual inspection and that its fluorescence intensity gradually increased with the increase in virus concentration. In accordance with the calibration curve (Fig. 6(b)), we found that the LOD of GO@TQD-LFA for inactivated SARS-CoV-2 virions was 609 copies/mL (387, 849 times dilution). Generally speaking, the SARS-CoV-2 viral loads of the respiratory tract specimens were higher than 10^5–10^6 copies/mL [44, 45]. Therefore, the sensitivity of our proposed GO@TQD-LFA is sufficient to meet the requirements for SARS-CoV-2 antigen testing in respiratory tract specimens.

Table 1 Recovery efficiency of SARS-CoV-2 NP, HAdV, and H1N1 virions detected in saliva samples using GO@TQD-LFA

Target	Added concentration	Detected concentration	Recovery (%)	CV (%)
SARS-CoV-2 NP (ng/mL)	5	4.65	93.1	7.39
	1	0.98	98.2	8.11
	0.1	0.10	100.1	4.15
HAdV (copies/mL)	5×10^5	5.42×10^5	108.4	4.44
	10^5	0.96×10^5	96.1	6.15
	10^4	1.03×10^4	103.4	4.56
H1N1 (copies/mL)	5×10^5	4.58×10^5	91.6	5.08
	10^5	1.03×10^5	102.7	7.01
	10^4	1.08×10^4	108.5	4.17

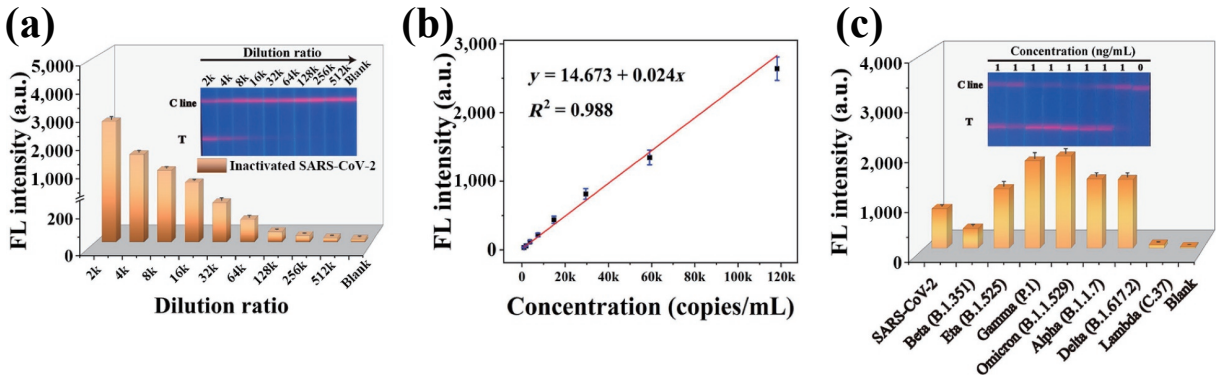

Figure 6 (a) Fluorescence photos and corresponding signal intensities of GO@TQD-LFA for different concentrations of inactivated SARS-CoV-2. (b) Calibration curves of GO@TQD-based LFA for inactivated SARS-CoV-2 samples. (c) Fluorescence photos and corresponding T line intensities for multiple SARS-CoV-2 NP variant strains.

Table 2 Comparison of the performances of the proposed assay and other recently reported LFA methods for respiratory virus detection

Signal mode	Target virus	LODs	Assay time	References
SERS-LFA	H1N1, HAdV	50 pfu/mL, 10 pfu/mL	30 min	[46]
Colorimetric-LFA	SARS-CoV-2	0.65 ng/mL	20 min	[47]
Chemiluminescence-LFA	SARS-CoV-2	0.1 ng/mL	16 min	[32]
Colorimetric-LFA	SARS-CoV-2	1.8×10^5 copies/mL	20 min	[48]
Colorimetric-LFA	SARS-CoV-2	2 ng/mL	20 min	[49]
Fluorescent-LFA	SARS-CoV-2	1 pg/mL	35 min	[43]
Dual signal-LFA	SARS-CoV-2	33 pg/mL	30 min	[50]
Colorimetric-LFA	SARS-CoV-2	38 pg/mL	10 min	[51]
Fluorescent-LFA	SARS-CoV-2	10 pg/mL	15 min	[34]
Fluorescent-LFA	SARS-CoV-2, H1N1, HAdV	8 pg/mL, 488 copies/mL, 471 copies/mL	15 min	This work

Considering that multiple SARS-CoV-2 variants, such as delta and omicron, have emerged and are still spreading rapidly worldwide, the identification ability of our method for these variants should be evaluated. Seven major variant strains of SARS-CoV-2 NP, including alpha (B.1.1.7), beta (B.1.351), eta (B.1.525), lambda (C.37), gamma (P.1), delta (B.1.617.2), and omicron (B.1.1.529), were purchased from Sino Biological Inc. and detected by using the proposed LFA method. As illustrated in Fig. 6(c), the proposed assay could well identify the six variant strains of SARS-CoV-2 NP, including omicron (B.1.1.529), at the concentration of 1 ng/mL but could not distinctly recognize lambda (C.37) under the same conditions. Moreover, the fluorescence intensity of some mutant strain groups was even higher than that of the wild-type SARS-CoV-2, suggesting the feasibility and great potential of our method for the direct detection of SARS-CoV-2 variants. We noticed that the GO@TQD based-LFA exhibited obvious advantages, including greater testing throughput, faster detection, and higher sensitivity, compared with recently reported highly sensitive LFA biosensors for respiratory virus detection (Table 2). The combination of the film-like GO@TQD tags and LFA platform contributes to the improvement in the performance of current POCT methods. Finally, the prepared GO@TQD-LFA strip can be well preserved in a vacuum-sealed plastic bag and maintains stable performance after storage for three months (Fig. S17 in the ESM). Thus, the GO@TQD-based LFA has great potential to be developed into a commercial detection reagent.

4 Conclusions

We proposed a 3D film-type GO@TQD fluorescent nanofilm with three layers of QD shells that was specially tailored for a multiplex LFA system for the ultrasensitive and simultaneous screening of three target respiratory viruses in complex biological specimens. Three layers of dense CdSe@ZnS-COOH QDs were successively coated onto the surfaces of 2D monolayer GO sheets via electrostatic adsorption-mediated LbL assembly. This approach transformed the 2D nanostructure into the 3D fluorescent nanofilm and provided larger surface areas, higher fluorescence signals, and better dispersibility and stability than the use of traditional spherical fluorescent tags for LFA detection. By introducing the film-type GO@TQD into LFA strips, the proposed assay can directly and simultaneously detect SARS-CoV-2, H1N1, and HAdV in 15 min with LODs of 8 ng/mL, 488 copies/mL, and 471 copies/mL, respectively. The sensitivity of GO@TQD-based LFA had improved by approximately 100 and 13 times that of traditional AuNP-based LFA and commercial QD bead-based LFA, respectively, and by over 12 times that of ELISA analysis. In addition, the GO@TQD-LFA exhibited excellent performance in the detection of real respiratory tract samples and most of SARS-CoV-2 mutant variants. Therefore, it has great practical potential for the rapid screening of respiratory viral infections and controlling the COVID-19 pandemic.

Acknowledgements

This study was supported by the National Natural Science Foundation of China (Nos. 81830101 and 32200076), the National Science and Technology Major Project for Infectious Diseases Control (Nos. 2018ZX10712001-010 and 2018ZX10101003-001), and the Natural Science Foundation of Anhui Province (No. 2208085MB29). The authors would like to thank Prof. Chengfeng Qin from Beijing Institute of Microbiology and Epidemiology for providing inactivated SARS-CoV-2 virions, and thank Ms. Le Zhao of National Center for Nanoscience and Technology for helping to conduct SEM analysis.

Electronic Supplementary Material: Supplementary material (Section S1 Experimental section, Section S2 Calculation of the maximum number of QDs on the GO@TQD nanofilm, Section S3 Optimization of the LFA method, and Figs. S1–S17 mentioned in the main text) is available in the online version of this article at https://doi.org/10.1007/s12274-022-5043-6.

References

[1] Shuai, H. P.; Chan, J. F. W.; Hu, B. J.; Chai, Y.; Yuen, T. T. T.; Yin, F. F.; Huang, X. E.; Yoon, C.; Hu, J. C.; Liu, H. et al. Attenuated replication and pathogenicity of SARS-CoV-2 B.1.1.529 Omicron. *Nature* **2022**, *603*, 693–699.

[2] Li, Q.; Guan, X. H.; Wu, P.; Wang, X. Y.; Zhou, L.; Tong, Y. Q.; Ren, R. Q.; Leung, K. S. M.; Lau, E. H. Y.; Wong, J. Y. et al. Early transmission dynamics in Wuhan, China, of novel coronavirus-infected pneumonia. *N. Engl. J. Med.* **2020**, *382*, 1199–1207.

[3] Wang, C. W.; Yang, X. S.; Gu, B.; Liu, H. F.; Zhou, Z. H.; Shi, L. L.; Cheng, X. D.; Wang, S. Q. Sensitive and simultaneous detection of SARS-CoV-2-specific IgM/IgG using lateral flow immunoassay based on dual-mode quantum dot nanobeads. *Anal. Chem.* **2020**, *92*, 15542–15549.

[4] Suleman, S.; Shukla, S. K.; Malhotra, N.; Bukkitgar, S. D.; Shetti, N. P.; Pilloton, R.; Narang, J.; Nee Tan, Y.; Aminabhavi, T. M. Point of care detection of COVID-19: Advancement in biosensing and diagnostic methods. *Chem. Eng. J.* **2021**, *414*, 128759.

[5] Leong, S. X.; Leong, Y. X.; Tan, E. X.; Sim, H. Y. F.; Koh, C. S. L.; Lee, Y. H.; Chong, C.; Ng, L. S.; Chen, J. R. T.; Pang, D. W. C. et al. Noninvasive and point-of-care surface-enhanced Raman scattering (SERS)-based breathalyzer for mass screening of coronavirus disease 2019 (COVID-19) under 5 min. *ACS Nano* **2022**, *16*, 2629–2639.

[6] Wu, X. J.; Cai, Y.; Huang, X.; Yu, X.; Zhao, L.; Wang, F.; Li, Q. G.; Gu, S. C.; Xu, T.; Li, Y. J. et al. Co-infection with SARS-CoV-2 and influenza A virus in patient with pneumonia, China. *Emerg. Infect. Dis.* **2020**, *26*, 1324–1326.

[7] Krumbein, H.; Kümmel, L. S.; Fragkou, P. C.; Thölken, C.; Hünerbein, B. L.; Reiter, R.; Papathanasiou, K. A.; Renz, H.; Skevaki, C. Respiratory viral co-infections in patients with COVID-19 and associated outcomes: A systematic review and meta-analysis. *Rev. Med. Virol.*, in press, https://doi.org/10.1002/rmv.2365.

[8] Kinoshita, T.; Watanabe, K.; Sakurai, Y.; Nishi, K.; Yoshikawa, R.; Yasuda, J. Co-infection of SARS-CoV-2 and influenza virus causes more severe and prolonged pneumonia in hamsters. *Sci. Rep.* **2021**, *11*, 21259.

[9] Cui, F. Y.; Zhou, H. S. Diagnostic methods and potential portable biosensors for coronavirus disease 2019. *Biosens. Bioelectron.* **2020**, *165*, 112349.

[10] Kevadiya, B. D.; Machhi, J.; Herskovitz, J.; Oleynikov, M. D.; Blomberg, W. R.; Bajwa, N.; Soni, D.; Das, S.; Hasan, M.; Patel, M. et al. Diagnostics for SARS-CoV-2 infections. *Nat. Mater.* **2021**, *20*, 593–605.

[11] Ji, T. X.; Liu, Z. W.; Wang, G. Q.; Guo, X. G.; Akbar Khan, S.; Lai, C. C.; Chen, H. Y.; Huang, S. W.; Xia, S. M.; Chen, B. et al. Detection of COVID-19: A review of the current literature and future perspectives. *Biosens. Bioelectron.* **2020**, *166*, 112455.

[12] Parolo, C.; Sena-Torralba, A.; Bergua, J. F.; Calucho, E.; Fuentes-Chust, C.; Hu, L. M.; Rivas, L.; Álvarez-Diduk, R.; Nguyen, E. P.; Cinti, S. et al. Tutorial: Design and fabrication of nanoparticle-based lateral-flow immunoassays. *Nat. Protoc.* **2020**, *15*, 3788–3816.

[13] Wang, L. Y.; Wang, X. K.; Cheng, L.; Ding, S. S.; Wang, G. Q.; Choo, J.; Chen, L. X. SERS-based test strips: Principles, designs and applications. *Biosens. Bioelectron.* **2021**, *189*, 113360.

[14] Huang, L.; Zhang, Y. X.; Liao, T.; Xu, K.; Jiang, C. X.; Zhuo, D.; Wang, Y.; Wen, H. M.; Wang, J.; Ao, L. J. et al. Compact magneto-fluorescent colloids by hierarchical assembly of dual-components in radial channels for sensitive point-of-care immunoassay. *Small* **2021**, *17*, e2100862.

[15] Bai, F. E.; Bu, T.; Zhao, S.; He, K. Y.; Zhang, H.; Li, R. X.; Li, M. Y.; Wang, Y.; Wang, L. Golf-shaped Bi_2Se_3 microparticles based-immunochromatographic strip for ultrasensitive detection of acetamiprid. *J. Hazard. Mater.* **2022**, *433*, 128810.

[16] Wang, X. K.; Choi, N.; Cheng, Z. Y.; Ko, J.; Chen, L. X.; Choo, J. Simultaneous detection of dual nucleic acids using a SERS-based lateral flow assay biosensor. *Anal. Chem.* **2017**, *89*, 1163–1169.

[17] Zhou, Y. F.; Chen, Y.; Liu, Y.; Fang, H.; Huang, X. L.; Leng, Y. K.; Liu, Z. Q.; Hou, L.; Zhang, W.; Lai, W. H. et al. Controlled copper *in situ* growth-amplified lateral flow sensors for sensitive, reliable, and field-deployable infectious disease diagnostics. *Biosens. Bioelectron.* **2021**, *171*, 112753.

[18] Zhang, Y.; Yu, Y.; Ying, J. Y. Multi-color Au/Ag nanoparticles for multiplexed lateral flow assay based on spatial separation and color co-localization. *Adv. Funct. Mater.* **2022**, *32*, 2109553.

[19] Yao, L. L.; Zhu, W. T.; Shi, J. B.; Xu, T. L.; Qu, G. B.; Zhou, W. H.; Yu, X. F.; Zhang, X. J.; Jiang, G. B. Detection of coronavirus in environmental surveillance and risk monitoring for pandemic control. *Chem. Soc. Rev.* **2021**, *50*, 3656–3676.

[20] Zhang, Z. W.; Ma, P.; Ahmed, R.; Wang, J.; Akin, D.; Soto, F.; Liu, B. F.; Li, P. W.; Demirci, U. Advanced point-of-care testing technologies for human acute respiratory virus detection. *Adv. Mater.* **2022**, *34*, e2103646.

[21] Ince, B.; Sezgintürk, M. K. Lateral flow assays for viruses diagnosis: Up-to-date technology and future prospects. *Trends Analyt. Chem.* **2022**, *157*, 116725.

[22] Zhu, X. H.; Zhang, Y. Y.; Liu, M. L.; Liu, Y. 2D titanium carbide MXenes as emerging optical biosensing platforms. *Biosens. Bioelectron.* **2021**, *171*, 112730.

[23] Lin, C. L.; Liang, S. S.; Peng, Y. S.; Long, L.; Li, Y. Y.; Huang, Z. R.; Long, N. V.; Luo, X. Y.; Liu, J. J.; Li, Z. Y. et al. Visualized SERS imaging of single molecule by Ag/black phosphorus nanosheets. *Nanomicro Lett.* **2022**, *14*, 75.

[24] Bu, T.; Jia, P.; Sun, X. Y.; Liu, Y. N.; Wang, Q. Z.; Wang, L. Hierarchical molybdenum disulfide nanosheets based lateral flow immunoassay for highly sensitive detection of tetracycline in food samples. *Sens. Actuators B Chem.* **2020**, *320*, 128440.

[25] Chen, M. P.; Liu, D.; Du, X. Y.; Lo, K. H.; Wang, S. P.; Zhou, B. P.; Pan, H. 2D materials: Excellent substrates for surface-enhanced Raman scattering (SERS) in chemical sensing and biosensing. *Trends Analyt. Chem.* **2020**, *130*, 115983.

[26] Zamora-Gálvez, A.; Morales-Narváez, E.; Romero, J.; Merkoçi, A. Photoluminescent lateral flow based on non-radiative energy transfer for protein detection in human serum. *Biosens. Bioelectron.* **2018**, *100*, 208–213.

[27] Ren, S. Y.; Li, Q. F.; Wang, J. Y.; Fan, B. Y.; Bai, J. L.; Peng, Y.; Li, S.; Han, D. P.; Wu, J.; Wang, J. et al. Development of a fast and ultrasensitive black phosphorus-based colorimetric/photothermal dual-readout immunochromatography for determination of norfloxacin in tap water and river water. *J. Hazard. Mater.* **2021**, *402*, 123781.

[28] Cheng, X. D.; Zheng, S.; Wang, W. Q.; Han, H.; Yang, X. S.; Shen, W. Z.; Wang, C. W.; Wang, S. Q. Synthesis of two-dimensional graphene oxide-fluorescent nanoprobe for ultrasensitive and multiplex immunochromatographic detection of respiratory bacteria. *Chem. Eng. J.* **2021**, *426*, 131836.

[29] Zheng, S.; Wang, C. G.; Li, J. X.; Wang, W. Q.; Yu, Q.; Wang, C. W.; Wang, S. Q. Graphene oxide-based three-dimensional Au nanofilm with high-density and controllable hotspots: A powerful film-type SERS tag for immunochromatographic analysis of multiple mycotoxins in complex samples. *Chem. Eng. J.* **2022**, *448*, 137760.

[30] Sasisekharan, V.; Pentakota, N.; Jayaraman, A.; Tharakaraman, K.; Wogan, G. N.; Narayanasami, U. Orthogonal immunoassays for IgG antibodies to SARS-CoV-2 antigens reveal that immune response lasts beyond 4 mo post illness onset. *Proc. Natl. Acad. Sci. USA* **2021**, *118*, e2021615118.

[31] Wang, P. F.; Nair, M. S.; Liu, L. H.; Iketani, S.; Luo, Y.; Guo, Y. C.; Wang, M.; Yu, J.; Zhang, B. S.; Kwong, P. D. et al. Antibody resistance of SARS-CoV-2 variants B.1.351 and B.1.1.7. *Nature* **2021**, *593*, 130–135.

[32] Liu, D.; Ju, C. H.; Han, C.; Shi, R.; Chen, X. H.; Duan, D. M.; Yan,

J. H.; Yan, X. Y. Nanozyme chemiluminescence paper test for rapid and sensitive detection of SARS-CoV-2 antigen. *Biosens. Bioelectron.* **2021**, *173*, 112817.

[33] Fabiani, L.; Saroglia, M.; Galatà, G.; De Santis, R.; Fillo, S.; Luca, V.; Faggioni, G.; D'Amore, N.; Regalbuto, E.; Salvatori, P. et al. Magnetic beads combined with carbon black-based screen-printed electrodes for COVID-19: A reliable and miniaturized electrochemical immunosensor for SARS-CoV-2 detection in saliva. *Biosens. Bioelectron.* **2021**, *171*, 112686.

[34] Hu, R. B.; Liao, T.; Ren, Y.; Liu, W. M.; Ma, R.; Wang, X. Y.; Lin, Q. H.; Wang, G. X.; Liang, Y. Y. Sensitively detecting antigen of SARS-CoV-2 by NIR-II fluorescent nanoparticles. *Nano Res.* **2022**, *15*, 7313–7319.

[35] Wang, C. W.; Xiao, R.; Wang, S.; Yang, X. S.; Bai, Z. K.; Li, X. Y.; Rong, Z.; Shen, B. F.; Wang, S. Q. Magnetic quantum dot based lateral flow assay biosensor for multiplex and sensitive detection of protein toxins in food samples. *Biosens. Bioelectron.* **2019**, *146*, 111754.

[36] Wang, C. W.; Yang, X. S.; Zheng, S.; Cheng, X. D.; Xiao, R.; Li, Q. J.; Wang, W. Q.; Liu, X. X.; Wang, S. Q. Development of an ultrasensitive fluorescent immunochromatographic assay based on multilayer quantum dot nanobead for simultaneous detection of SARS-CoV-2 antigen and influenza A virus. *Sens. Actuators B Chem.* **2021**, *345*, 130372.

[37] Zheng, S.; Wu, T.; Li, J. X.; Jin, Q.; Xiao, R.; Wang, S. Q.; Wang, C. W. Difunctional immunochromatographic assay based on magnetic quantum dot for ultrasensitive and simultaneous detection of multiple mycotoxins in foods. *Sens. Actuators B Chem.* **2022**, *359*, 131528.

[38] Wang, C. W.; Wang, C. G.; Li, J. X.; Tu, Z. J.; Gu, B.; Wang, S. Q. Ultrasensitive and multiplex detection of four pathogenic bacteria on a bi-channel lateral flow immunoassay strip with three-dimensional membrane-like SERS nanostickers. *Biosens. Bioelectron.* **2022**, *214*, 114525.

[39] Shen, W. Z.; Wang, C. G.; Zheng, S.; Jiang, B.; Li, J. X.; Pang, Y. F.; Wang, C. W.; Hao, R. Z.; Xiao, R. Ultrasensitive multichannel immunochromatographic assay for rapid detection of foodborne bacteria based on two-dimensional film-like SERS labels. *J. Hazard. Mater.* **2022**, *437*, 129347.

[40] Wang, C. W.; Shen, W. Z.; Rong, Z.; Liu, X. X.; Gu, B.; Xiao, R.; Wang, S. Q. Layer-by-layer assembly of magnetic-core dual quantum dot-shell nanocomposites for fluorescence lateral flow detection of bacteria. *Nanoscale* **2020**, *12*, 795–807.

[41] Gao, F.; Lei, C.; Liu, Y.; Song, H.; Kong, Y. Q.; Wan, J. J.; Yu, C. Z. Rational design of dendritic mesoporous silica nanoparticles' surface chemistry for quantum dot enrichment and an ultrasensitive lateral flow immunoassay. *ACS Appl. Mater. Interfaces* **2021**, *13*, 21507–21515.

[42] Wang, J.; Jiang, C. X.; Jin, J. N.; Huang, L.; Yu, W. B.; Su, B.; Hu, J. Ratiometric fluorescent lateral flow immunoassay for point-of-care testing of acute myocardial infarction. *Angew. Chem., Int. Ed.* **2021**, *60*, 13042–13049.

[43] Wang, C. W.; Cheng, X. D.; Liu, L. Y.; Zhang, X. C.; Yang, X. S.; Zheng, S.; Rong, Z.; Wang, S. Q. Ultrasensitive and simultaneous detection of two specific SARS-CoV-2 antigens in human specimens using direct/enrichment dual-mode fluorescence lateral flow immunoassay. *ACS Appl. Mater. Interfaces* **2021**, *13*, 40342–40353.

[44] Pan, Y.; Zhang, D. T.; Yang, P.; Poon, L. L. M.; Wang, Q. Y. Viral load of SARS-CoV-2 in clinical samples. *Lancet Infect. Dis.* **2020**, *20*, 411–412.

[45] Layden, J. E.; Ghinai, I.; Pray, I.; Kimball, A.; Layer, M.; Tenforde, M. W.; Navon, L.; Hoots, B.; Salvatore, P. P.; Elderbrook, M. et al. Pulmonary illness related to e-cigarette use in Illinois and Wisconsin—Final report. *N. Engl. J. Med.* **2020**, *382*, 903–916.

[46] Wang, C. W.; Wang, C. G.; Wang, X. L.; Wang, K. L.; Zhu, Y. H.; Rong, Z.; Wang, W. Y.; Xiao, R.; Wang, S. Q. Magnetic SERS strip for sensitive and simultaneous detection of respiratory viruses. *ACS Appl. Mater. Interfaces* **2019**, *11*, 19495–19505.

[47] Grant, B. D.; Anderson, C. E.; Williford, J. R.; Alonzo, L. F.; Glukhova, V. A.; Boyle, D. S.; Weigl, B. H.; Nichols, K. P. SARS-CoV-2 coronavirus nucleocapsid antigen-detecting half-strip lateral flow assay toward the development of point of care tests using commercially available reagents. *Anal. Chem.* **2020**, *92*, 11305–11309.

[48] Lee, J. H.; Choi, M.; Jung, Y.; Lee, S. K.; Lee, C. S.; Kim, J.; Kim, J.; Kim, N. H.; Kim, B. T.; Kim, H. G. A novel rapid detection for SARS-CoV-2 spike 1 antigens using human angiotensin converting enzyme 2 (ACE2). *Biosens. Bioelectron.* **2021**, *171*, 112715.

[49] Kim, H. Y.; Lee, J. H.; Kim, M. J.; Park, S. C.; Choi, M.; Lee, W.; Ku, K. B.; Kim, B. T.; Changkyun Park, E.; Kim, H. G. et al. Development of a SARS-CoV-2-specific biosensor for antigen detection using scFv-Fc fusion proteins. *Biosens. Bioelectron.* **2021**, *175*, 112868.

[50] Han, H.; Wang, C. W.; Yang, X. S.; Zheng, S.; Cheng, X. D.; Liu, Z. Z.; Zhao, B. H.; Xiao, R. Rapid field determination of SARS-CoV-2 by a colorimetric and fluorescent dual-functional lateral flow immunoassay biosensor. *Sens. Actuators B Chem.* **2022**, *351*, 130897.

[51] Oh, H. K.; Kim, K.; Park, J.; Im, H.; Maher, S.; Kim, M. G. Plasmon color-preserved gold nanoparticle clusters for high sensitivity detection of SARS-CoV-2 based on lateral flow immunoassay. *Biosens. Bioelectron.* **2022**, *205*, 114094.